RSC Advances

PAPER

View Article Online
View Journal | View Issue

Cite this: *RSC Adv.*, 2024, **14**, 2410

Synthesis of chitosan-based flocculant by dielectric barrier discharge modification and its flocculation performance in wastewater treatment†

Haixia Wu, * Wang Shen, Quanfa Zhao and Weiwei Zhang

Received 14th September 2023
Accepted 4th January 2024

DOI: 10.1039/d3ra06265a

rsc.li/rsc-advances

As a typical type of organic flocculant, chitosan is limited by its poor water solubility and narrow pH range application. Grafting modification can improve chitosan's solubility and availability through linking macromolecular chains with other types of water-soluble groups or functional side groups. In this study, dielectric barrier discharge (DBD) was used to active the surface of chitosan, then activated chitosan was polymerized with acrylamide to synthesize a chitosan-based flocculant, chitosan-acrylamide (CS-AM). During the synthesis of CS-AM, the optimal conditions were determined as follows: discharge time of 5 min, discharge power of 60 W, total monomer mass concentration of 80 g L^{-1}, polymerization time of 3 h, polymerization temperature of 70 °C, and *m*(CS) : *m*(AM) ratio of 1 : 3. The structure and morphological characteristics of CS-AM were investigated and analyzed by Fourier transform infrared (FTIR) spectroscopy, X-ray photoelectron spectroscopy (XPS), thermogravimetric (TG) analysis, scanning electron microscopy (SEM), X-ray diffraction (XRD) and N_2 physical adsorption, respectively. The removal efficiency of kaolin suspension and CNTs suspension can reach up to 95.9% and 90.2% after flocculation of CS-AM. Furthermore, the zeta potential of the supernatant from the CS-AM treated kaolin suspension at different pH values was examined, and the flocculation mechanism of CS-AM was analyzed. This study provides new ideas for the preparation and development of modified chitosan and broadens its application in water treatment.

Introduction

The flocculation method, which has the advantages of simplicity, cost-effectiveness, and high treatment efficiency, is widely used in sewage treatment processes.[1,2] Commonly used flocculants include iron salt, aluminum salt, silicate, and other inorganic flocculants, as well as natural organic polymer flocculants, synthetic organic polymer flocculants, and microbial flocculants. Among these natural organic polymer flocculants, chitosan (CS) is a typical example. It has good application prospect in the field of sewage treatment because of its safety, non-toxicity, biodegradation and environmental friendliness.[3] CS consists of randomly distributed beta-(1–4)-linked *N*-acetyl-D-glucosamine and D-glucosamine, which are obtained by deacetylation of chitin. Chitosan contains many reactive groups, such as amine and carboxyl groups, in its structure, and amino groups can generate a positive charge under acidic conditions, making it highly effective in removing negatively charged particles, heavy metals, and humic acid from sewage.[4–7] However, the application of chitosan is greatly limited by its poor water solubility, low mechanical strength, and narrow pH range.[3] Chitosan can be modified by substitution, oxidation, crosslinking and grafting to improve its solubility and availability.[8]

Thermal-induced polymerization, ultraviolet light-induced polymerization, microwave-induced polymerization, radiation-induced polymerization, and plasma-induced polymerization commonly result in the generation of chitosan.[9] For example, Chen utilized acrylamide (AM), methacrylate oxyethyl trimethylammonium chloride (DMC) as raw materials for polymerization to synthesize a new CS-modified flocculant, using UV-H_2O_2 initiation.[10] This flocculant exhibited superior flocculation ability compared to CS. In another study, Yu *et al.* employed acrylic acid and CS as raw materials and *N*,*N*′-methylene diacrylamide as a crosslinker to prepare a CS/polyacrylic acid (CS/PAA) hydrogel in an aqueous solution.[11] This hydrogel demonstrated excellent performance in terms of its properties.

Low-temperature plasma technology is a new advanced oxidation process widely used in environment protection.[12–17] Plasma-initiated graft polymerization allows the introduction of multifunctional groups onto the surface of substances without secondary contamination. The energy provided by the plasma activates polymerizable monomers to produce various active particles that collide with each other or with monomers and active particles, causing small molecular chains to form large molecular chains.[18] It offers several advantages over heat

College of Urban Construction, Nanjing Tech University, Nanjing 211816, China. E-mail: wuhaixia@njtech.edu.cn

† Electronic supplementary information (ESI) available. See DOI: https://doi.org/10.1039/d3ra06265a

generation, ultraviolet light initiation, and radiation initiation, including less chemicals, less pollution, high efficiency, green and environmental protection,[3] thereby presenting significant application potential.

In this study, a CS-AM flocculant was prepared by polymerizing CS with AM. The preparation conditions, such as discharge time, discharge power, total monomer concentration, polymerization temperature, polymerization time, and m(CS) : m(AM) mass ratio, were investigated. The CS-AM flocculant was characterized using Fourier transform infrared spectroscopy (FTIR), X-ray diffraction (XRD), thermogravimetric (TG) analysis, X-ray photoelectron spectroscopy (XPS), and scanning electron microscopy (SEM). Optimized preparation conditions were employed to synthesize CS-AM, which was then applied in the flocculation treatment of kaolin suspension and carbon nanotubes (CNTs) suspension. The flocculation performance of the CS-AM flocculant under different conditions was examined, and the zeta potential of the supernatant was explored. This study not only offers a novel approach for the preparation and advancement of modified CS but also introduces a new flocculant for wastewater treatment.

Experiment

Material

All chemicals used in this experiment were of analytical purity and used without any additional purification. CS (80–95% degree of deacetylation, 50–800 mPa s of viscosity), AM and ammonium persulfate were sourced from Shanghai Aladdin Biochemical Technology Co., LTD (Shanghai, China). Ultra-fine kaolin was obtained from Shanghai Maclin Biochemical Technology Co., LTD (Shanghai, China), and CNTs were purchased from Nanjing Sheng jian Quan Glass Instrument Co., LTD The experimental water was prepared using an ultrapure water machine (EPED-ER-10 TX, Nanjing Pu Yida Technology Development Co., LTD, China).

Preparation of CS-AM

A specific amount of CS was introduced into a dielectric barrier discharge (DBD) device (S1). The plasma generator's switch button was turned on, and the discharge power was adjusted before initiating the timing. Once the reaction was complete, the plasma generator was turned off. The treated CS was then transferred into a solution containing a certain concentration of AM. Subsequently, 20 mg of ammonium persulfate initiator was quickly added to the mixture, which was stirred in a water bath at a predetermined temperature for a duration of 1–6 h. The total mass of the monomers used was 80 g L^{-1}. Following the completion of the reaction, the CS-AM polymer gel was cooled to room temperature and rinsed with absolute ethanol. The resulting mixture was transferred to a centrifuge tube and subjected to centrifugation. After centrifugation, the polymer was dried at 80 °C and sieved through a 200 mesh screen.

Catkin experiment

To ensure the formation of a uniformly dispersed suspension, the kaolin and CNTs suspensions were subjected to 10 min of dispersion using an ultrasonic oscillator operating at 90 W and 20 kHz after preparation. For the flocculation experiment, 100 mL of the kaolin suspension or CNTs suspension was transferred to a beaker placed on a sixfold coagulation mixer. Without special instructions, the stirring intensity was set at 300 rad per min for 2 min at a fast speed, followed by 75 rad per min for 18 min at a slow speed. After stirring, the mixture was allowed to stand for 30 min, and the supernatant was collected for water sample analysis. The concentration of the kaolin suspension was determined using UV spectrophotometry at 341 nm, whereas the characteristic peak of CNTs at 262 nm served as the measurement index. Turbidity detection was performed using a meter (2100Q, HACH, USA). All experiments were repeated three times.

Methods for the characterization of the CS-AM

The FTIR profiles of CS and CS-AM were determined using a FTIR spectrometer (Nicolet iS20, Thermo Scientific, USA). The morphologies of CS, plasma-modified CS, and CS-AM were examined through imaging using a Czech TESCAN MIRA LMS scanning electron microscope (SEM). The surface element composition and functional groups of the samples were analyzed separately using an XPS (K-Alpha, Thermo Scientific, USA). X-ray diffractometry (Smartlab, Rigaku, Japan) was employed to investigate the crystal structures of CS and CS-AM. Thermogravimetric analysis of the samples was conducted using a synchronous thermal analyzer (STA-8000, PerkinElmer, USA) with a heating rate of 10 °C min^{-1} from 30 °C to 600 °C. The particle size distribution and system stability were characterized by analyzing the zeta potential using a zeta potential analyzer (Nano ZS90, Malvern Zetasizer, UK).

The discharge power P is calculated according to eqn (1) (ref. 3)

$$P = \frac{1}{T}\int_0^T U_t\left(I_t - I_t^{'}\right)\mathrm{d}t \quad (1)$$

where P is the discharge power (W); T is the discharge time (s); I_t is the current (A); $I_t^{'}$ is the displacement current (A); U_t is the voltage (V).

The grafting efficiency was calculated according to eqn (2) (ref. 19)

$$\text{Grafting efficiency } (\%) = \frac{W_2 - W_1}{W_1} \times 100\% \quad (2)$$

where W_1 and W_2 are the weights of original and grafted samples (g), respectively.

Results and analysis

Synthetic optimization of the CS-AM

Effects of discharge on the synthesis. The control conditions for the experiment were set as m(CS) : m(AM) = 1 : 2, with a polymerization temperature of 70 °C and a polymerization time of 3 h. The impact of plasma discharge time on the

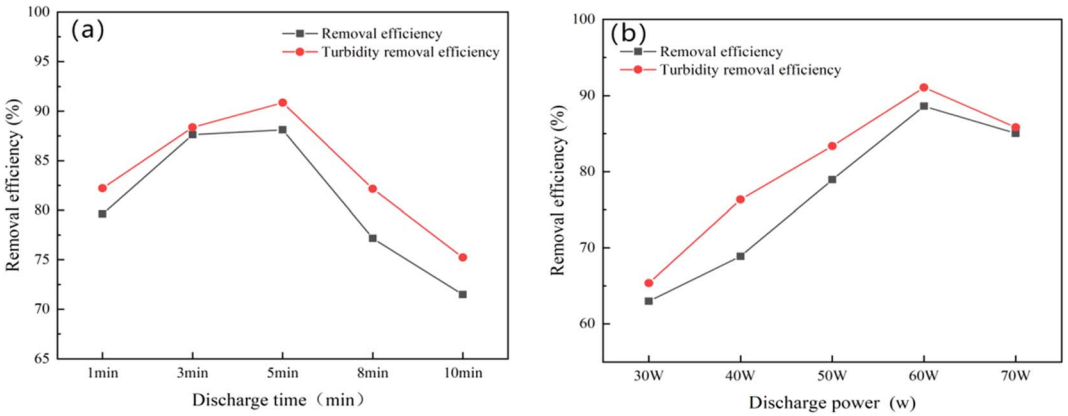

Fig. 1 Influence of (a) discharge time (discharge power of 60 W) and (b) discharge power (discharge time of 5 min) on the synthesized CS-AM for kaolin suspensions treatment (polymerization temperature of 70 °C, polymerization time of 3 h, CS to AM mass ratio of 1 : 2).

removal of kaolin suspension and turbidity by the synthesized CS-AM polymerization product is depicted in Fig. 1a. Notably, CS-AM synthesized with a discharge time of 5 min demonstrated the most effective flocculation of the kaolin suspension. Following plasma discharge treatment, the active free radicals on the surface of CS increased along with the formation of functional groups on the surface of CS-AM due to polymerization, thereby enhancing its flocculation properties. However, prolonged discharge time could potentially lead to structural damage and the disappearance of certain functional groups,[20,21] thereby resulting in a decline in the removal of the kaolin suspension by CS-AM.

Fig. 1b shows that the synthesized CS-AM exhibited the most effective flocculation of the kaolin suspension at a discharge power of 60 W. The lower the discharge power, the less free radical production, leading to a weaker subsequent polymerization grafting effect.[22] Conversely, as the discharge power increased, the electric field within the discharge region intensified, thereby facilitating the ionization of the gas and generating a higher quantity of active particles.[23] This phenomenon significantly promoted the grafting copolymerization reaction.[24] However, when the discharge power exceeded 60 W, the excess free radicals induced the homopolymerization of AM and CS.[25] In addition, the material experienced intensified etching, causing partial hole collapse, which was unfavorable for the subsequent grafting copolymerization reaction.

Effects of the CS to AM mass ratio on the synthesis. The impact of different CS to AM mass ratios (m(CS) : m(AM) = 2 : 3, 1 : 2, 2 : 5, 1 : 3, 1 : 4) on the synthesized polymer products and their turbidity is presented in Fig. 2. At m(CS) : m(AM) = 1 : 3, the CS-AM exhibited a 91.1% removal efficiency of the kaolin suspension and a 92.0% reduction in turbidity. The CS to AM mass ratio plays a role in the diffusion rate of CS monomers into AM and their dispersion within AM. When the m(CS) : m(AM) is high, the active sites on CS may not be efficiently utilized. As the mass proportion of AM increases, the concentration in the reaction system rises, leading to an increased collision between AM and CS molecules and subsequently enhancing the grafting efficiency. Nevertheless, if the concentration of AM is too high, the homopolymerization reaction will occur and the flocculation performance will be reduced.[26] Thus, a suitable CS to AM mass ratio for synthesizing CS-AM is determined to be 1 : 3.

The internal structure character of the flocculant also has an effect on the flocculation performance.[27] When the mass ratio of CS to AM is 1 : 3, the grafting efficiency is 75.6%. It is necessary for CS-AM to have a proper chitosan grafting efficiency. Enough CS and AM content in CS-AM can greatly enhance its charge neutralization ability, and completely neutralize more negatively charged Kaolin particles. However, excessive CS in CS-AM will have a negative effect. This is mainly because the active reaction energy of AM and CS monomers is higher than CS, and the steric hindrance is relatively small. It leads to a decrease in the molecular weight of the synthesized CS-AM, which is not conducive to the occurrence of adsorption bridging.[28]

Effects of the polymerization time and temperature on the synthesis. The impact of polymerization temperature on the

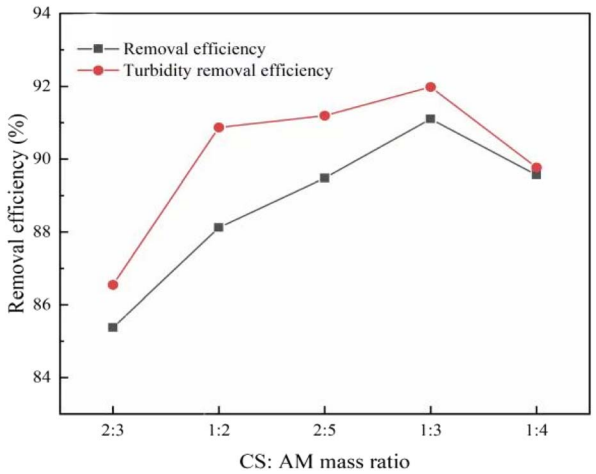

Fig. 2 Influence of m(CS) : m(AM) on the synthesized CS-AM for kaolin suspension treatment (discharge time of 5 min, discharge power of 60 W, polymerization temperature of 70 °C, polymerization time of 3 h).

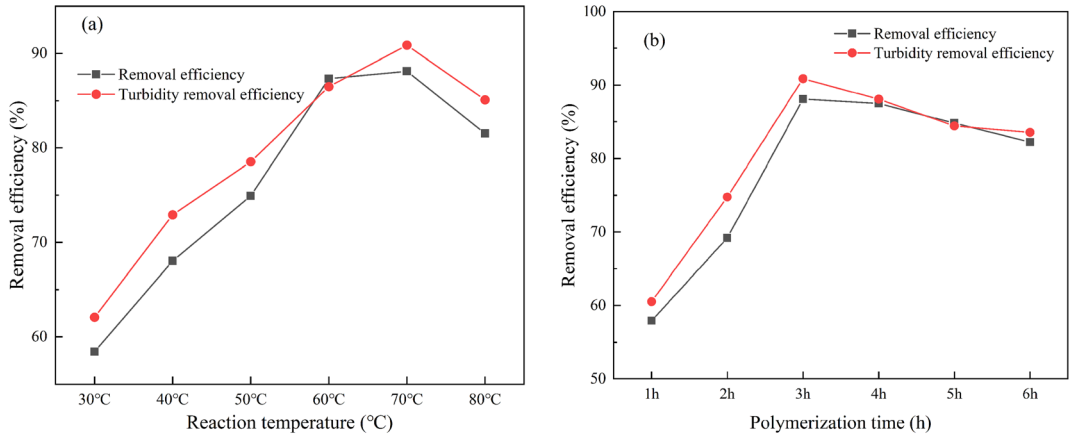

Fig. 3 Influence of (a) polymerization temperature (polymerization time of 3 h) and (b) polymerization time (polymerization temperature of 70 °C) on the synthesized CS-AM for kaolin suspensions (discharge time of 5 min, discharge power of 60 W, CS to AM mass ratio of 1 : 2).

removal of kaolin suspension by CS-AM is illustrated in Fig. 3a. The polymerization temperature exerts a substantial influence on the removal of the kaolin suspension and its turbidity by CS-AM. As the polymerization temperature increases, the removal of the kaolin suspension and turbidity shows a significant improvement. However, beyond a polymerization temperature of 70 °C, the removal begins to decline. Thus, the optimal polymerization temperature for achieving the highest removal efficiency is determined to be 70 °C.

When the polymerization temperature is low, the transfer and diffusion rate of active free radicals is correspondingly low. AM molecule cannot combine well with the active site on CS, which will lead to low graft copolymerization efficiency and poor graft effect.[29] Increasing temperature enhances the possibility of collision between active radicals and monomers, thereby accelerating the chain growth reaction and facilitating graft copolymerization.[30] However, excessively high temperatures are detrimental to the graft copolymerization reaction primarily due to the increased viscosity of the reaction system, which hinders the spread of monomers to the active grafting sites. The polymerization ability of the amino and hydroxyl groups on the chitosan chain decreases when the temperature is too high.[31] It can negatively affect homopolymerization, chain conversion and chain termination rates. High temperature will also cause crosslinking reaction, which will ultimately affect the effect of CS-AM in removing kaolin suspension and its turbidity.

The effects of polymerization time on the removal of kaolin suspension by CS-AM is depicted in Fig. 3b. As the polymerization time increases, the removal of kaolin suspension and turbidity initially increases and then decreases. The optimal removal rates of 88.1% and 90.9% were achieved for kaolin suspension and turbidity at a polymerization time of 3 h, respectively.

A shorter reaction time results in insufficient interaction between the active groups and monomers, leading to incomplete polymerization. After a certain time, the polymerization reaction between monomers is completed, and the influence on the grafting efficiency is small.[32] An excessively long reaction time depletes the available reactive groups, increases the viscosity of the reaction system, and may induce side reactions and chain transfer.[33] As a consequence, the grafting efficiency may no longer increase or even slightly decrease.

Characterization of the CS-AM

FT-IR analysis. The FTIR spectra of CS, plasma-modified CS, CS-AM, and AM were analyzed to determine the structure of plasma-modified CS and CS-based flocculant. Fig. 4 presents the results, revealing multiple characteristic absorption peaks at different wavelengths for each substance. For CS and plasma-modified CS, the characteristic absorption peak near 1081 cm^{-1} corresponds to the stretching vibration of the primary alcohol (C–OH) group. The peak near 1389 cm^{-1} indicates the stretching vibration of the amide (CN) group, while the peak near 1648 cm^{-1} corresponds to the stretching vibration of the primary amine (N–H) group. The peak near 2882 cm^{-1} represents the expansion vibration of the carbon and hydrogen bond (C–H), and the peak

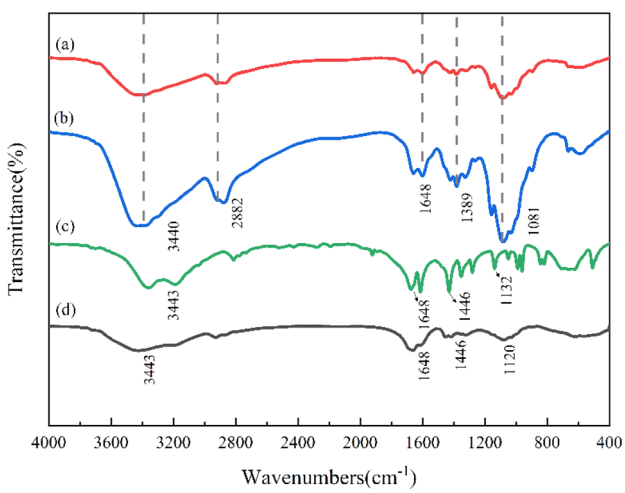

Fig. 4 FTIR spectra: (a) CS; (b) plasma modified CS (60 W, 5 min); (c) AM; (d) CS-AM (60 W, 5 min, m(CS) : m(AM) = 1 : 2, 3 h, 70 °C).

near 3440 cm^{-1} corresponds to the expansion vibration of the amino ($-NH_2$) or hydroxyl (–OH) group.[22,34,35] Compared with untreated CS, the characteristic peaks of CS after air plasma treatment are more pronounced, with stronger stretching vibrations of the groups. This observation can be attributed to the introduction of a significant number of oxygen-containing functional groups and active groups on the CS surface during the plasma treatment.[36,37] In the infrared spectrum of AM, the absorption peaks at 3443, 1648, 1446, and 1132 cm^{-1} represent the mid-NH_2, C=O, C–N, and C–O groups, respectively. The proximity of the absorption peaks near 3443, 1648, 1446, and 1120 cm^{-1} may indicate the overlap of characteristic absorption peaks resulting from the introduction of AM.[21,23] Based on the comparative analysis of polymer spectra, the successful synthesis of CS-AM is demonstrated.

SEM analysis. Fig. 5 illustrates the surface morphology of CS before and after plasma treatment, as well as the surface morphology of synthetic CS-AM. Without plasma treatment, the CS surface appears smooth. However, after discharge plasma treatment, the CS surface exhibits uniform concave points and an "orange peel" texture, indicating some degree of etching on the CS surface. AM has a network structure. The synthesized CS-AM shows a significant change in surface morphology, with increased surface roughness and irregularity. Many large

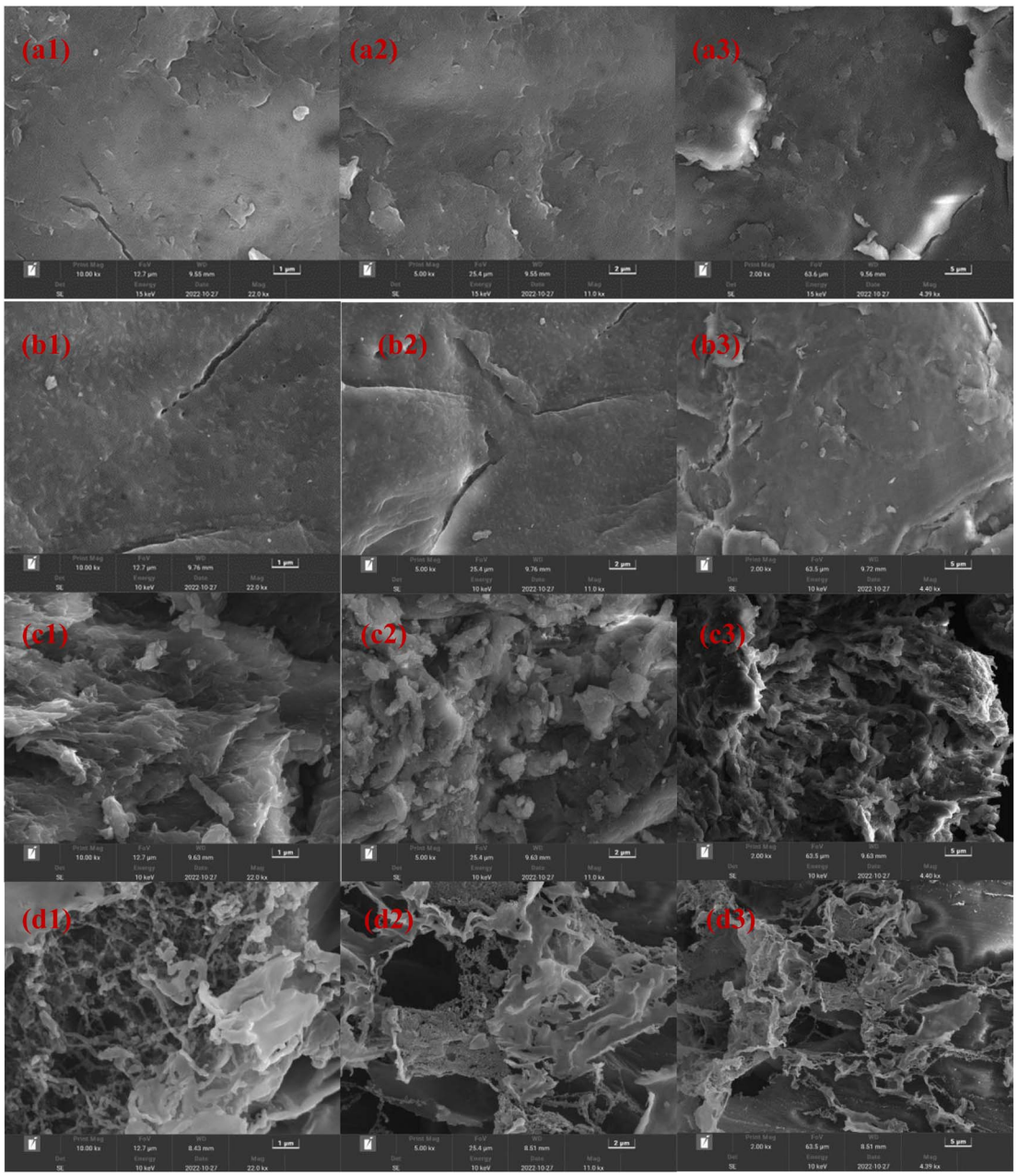

Fig. 5 SEM of (a) CS; (b) plasma modified CS (60 W, 5 min); (c) CS-AM (60 W, 5 min, m(CS) : m(AM) = 1 : 2, 3 h, 70 °C); (d) AM ((a1,b1,c1,d1) × 10.0k×, (a2,b2,c2,d2) × 5.0k×, (a3,b3,c3,d3) × 2.0k×).

porous and raised structures are present, providing a larger surface area. This feature facilitates the polymer's contact with the water environment, making it easier to interact with and capture colloidal particles.[38–40] As a result, the flocculation performance of CS-AM is greatly enhanced.

XPS analysis. The XPS full spectrum analysis (Fig. 6 and S2†) reveals the characteristic peaks for O 1s, C 1s, and N 1s in all four species at 284.6, 399.8, and 532.2 eV, respectively, indicating that the main elements present are C, N, and O.[41] The C 1s peak corresponds to C in C, plasma-modified CS, CS-AM, and AM, while the N 1s peak corresponds to N in CS, plasma-modified CS, and CS-AM. This instance indicates that the element and functional group content of the materials undergo changes after plasma treatment. Table 1 shows that the proportion of N and O elements increases in modified CS, while the proportion of grafted polymer CS-AM increases, resulting in a C/O ratio of 2.5%. Table S2† reveals changes in the content of C=O/O–C–O and amide groups after CS modification. Additionally, the content of C–C/C–H and NH_2 undergoes changes after grafting between CS and AM.

TG-DSC analysis. The TG-DSC is shown in Fig. 7. There are only two weight loss stages in the process of CS thermal decomposition: the first stage is 29.22–106.23 °C, and the weight loss rate is 7.7%; the second stage is 85.67–600 °C, and the weight loss rate is 54.87%. In addition, at 69.39 °C, the CS appeared an exothermic peak, and this part of the weight loss is mainly caused by the decomposition of chitosan in the oligoser state and water evaporation.[42] At 293.05 °C, an exothermic peak appeared, due to the CS crystal type transition during heat treatment.[43] There are two stages of weight loss in plasma modified CS: the first stage is 29.22–101.77 °C, and the loss rate is 4.18%; the second stage is 101.77–600 °C, and the loss rate is 58.18%. In addition, plasma modified CS showed exothermic peaks at 66.13 °C and 289.37 °C. The thermal weight-difference heat curves of CS and plasma modified CS are basically similar, but slightly different, indicating that the thermal stability of CS does not change much before and after modification, while the hydrophilic group introduced on the surface of the CS after plasma modification adsorbed more water, resulting in different water evaporation of weight loss.

The thermal decomposition of AM is divided into three main stages: the first stage, in the range of 30–167.3 °C, the weight loss rate is 2.14%, this stage is due to the heat loss caused by the water absorbed on the AM surface; In the second stage, the heat loss in the range of 167.3–600 °C and the thermal decomposition of the amide group of AM reaches 57.74%.[44,45] The comparison of the CS difference heat-thermal weight curve with the CS-AM difference heat-thermal weight curve can be found to be both similar and different. The difference is that the CS-AM thermal weight loss is divided into three stages (first stage: 28.82–128.31 °C, weight loss rate 10.77%; second stage: 128.31–347.99 °C, weight loss rate 25.28%; third stage: higher than 347.79–600 °C, weight loss rate 31.16%). At the temperature of 383.33 °C, there is an exothermic peak in the differential heat curve of CS-AM, which is due to the destruction of the original CS molecular structure after the introduction of AM monomer into the CS molecular chain, and the decomposition of the AM amide group and the thermal decomposition of the CS skeleton during the heat treatment. It can be inferred that CS-AM has good thermal stability and hardly decomposes by heating during routine use and storage.[46]

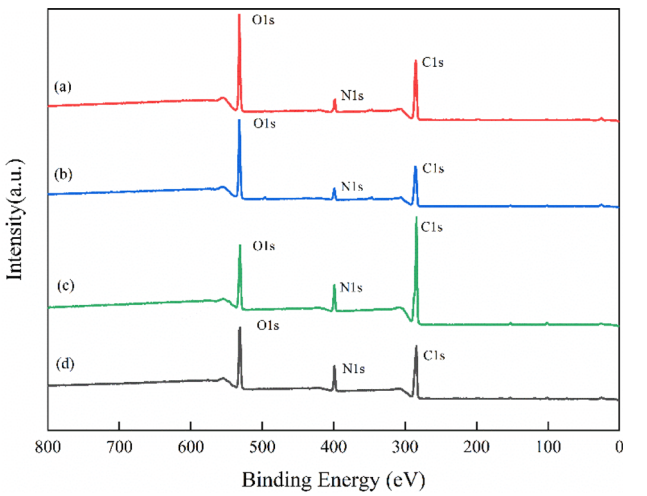

Fig. 6 XPS survey scans: (a) CS; (b) plasma modified CS (60 W, 5 min); (c) AM; (d) CS-AM (60 W, 5 min, m(CS) : m(AM) = 1 : 2, 3 h, 70 °C).

Table 1 Relative content of the elements C, N and O for the four substances

	The proportion of elements (%)			Element than (%)	
Sample	N	C	O	C/O	C/N
CS	6.49	64.68	28.83	2.24	9.97
Plasma modified CS	6.92	61.22	31.86	1.92	8.85
CS-AM	11.85	62.99	25.16	2.50	5.32
AM	8.88	73.86	17.26	4.28	8.32

XRD analysis. The XRD mapping results of the four species are presented in Fig. 8. A prominent diffraction peak at 2θ = 20.3 °C, which is a typical type II crystallinity, confirms the regular crystal structure of CS.[47] However, in the grafted copolymer CS-AM, the diffraction peak shows a weaker intensity compared with CS. Additionally, the peak exhibits broadening and a significant rightward shift, indicating a change in the crystal structure.[48] This change in the XRD diffraction pattern primarily occurs due to the introduction of AM molecules, which weaken the intermolecular hydrogen bonding in the CS structure. Consequently, the degree of crystallinity decreases, thereby affecting the order of the CS molecular chain and disrupting the original crystalline structure.[49,50] In conclusion, the XRD spectral results indicate that AM has been successfully grafted onto CS.

N_2 physical adsorption. The structural characteristics of CS-AM was analyzed by using nitrogen adsorption, desorption, and pore size analysis. As shown in Table S3,† the BET specific surface area of CS-AM is 0.6142 $m^2\ g^{-1}$ and the average pore size is 24.40 nm. The average pore size of raw CS is 58.3 nm, of the modified chitosan-pandan is 35.3 nm,[35] and of the chitosan graft poly developed by Jin *et al.* is 76.9–115.4 nm.[51] From this, it

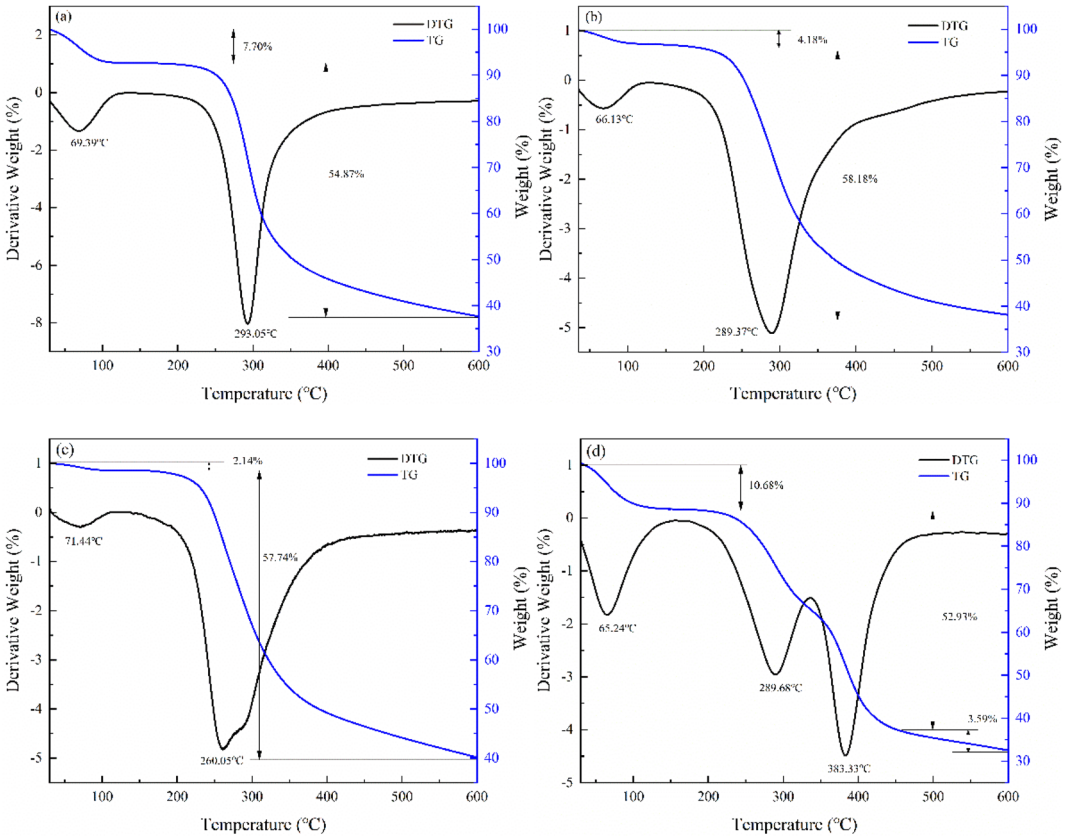

Fig. 7 TG-DSC graphs: (a) CS; (b) plasma modified CS (60 W, 5 min); (c) AM; (d) CS-AM (60 W, 5 min, *m*(CS) : *m*(AM) = 1 : 2, 3 h, 70 °C).

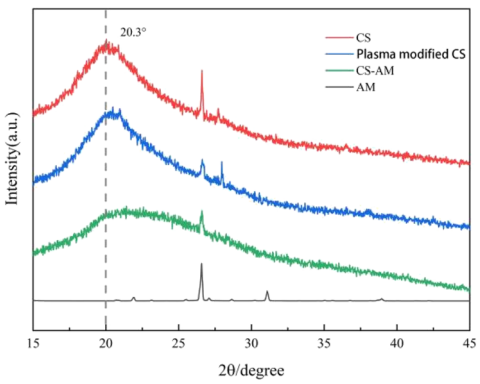

Fig. 8 XRD graphs (60 W, 5 min, *m*(CS) : *m*(AM) = 1 : 2, 3 h, 70 °C).

can be seen that the average pore size of chitosan-based flocculants is in the nanometer level. As shown in Fig. S3,† the CS-AM samples before and after adsorption exhibit a V-type adsorption desorption isotherm, indicating that mesopores dominate in the composite sphere (pore size between 2–50 nm).

Flocculation properties of CS-AM

Flocculation and removal effect of kaolin suspension. Fig. 9a illustrates the removal of kaolin suspension by CS-AM, CS, AM, and PAM at a dosage of 3 mg L^{-1}, with the order of effectiveness as follows: CS-AM > PAM > CS > AM. The polymerization product CS-AM exhibits the highest flocculation effect. The comparison of CS-AM with other flocculants is shown in Table S4.† The impact of CS-AM flocculant dosage on the removal is presented in Fig. 9b, where the optimal removal is achieved at a dosage of 5 mg L^{-1}. As the dosage increases, the flocculant's electric neutralization and adsorption bridging effects are strengthened, resulting in improved flocculation performance and higher removal rates of kaolin suspension and turbidity.[52] However, excessive addition of the flocculant leads to its adsorption on the surface of kaolin particles. This phenomenon causes repulsion between the positive charge of the flocculant and the polymer surface, resulting in re-stabilization and a decrease in turbidity removal to a certain extent.[53]

Fig. 9c depicts the impact of solution pH on the removal of kaolin suspension and turbidity. The pH value of the reaction system plays a vital role in wastewater flocculation. Optimal water treatment efficacy is achieved under acidic and neutral conditions, while alkaline environments result in a rapid decline in the removal of kaolin suspension and turbidity, which decreases with increasing pH value. The highest removal is observed at pH 7, reaching 96.9% and 95.8%. CS-AM contains amino groups, which are more easily protonated under acidic or neutral conditions. This finding enhances the flocculant's charge neutralization capacity, enabling effective charge neutralization of negatively charged kaolin particles. Additionally, in acidic or neutral conditions, the presence of hydrogen

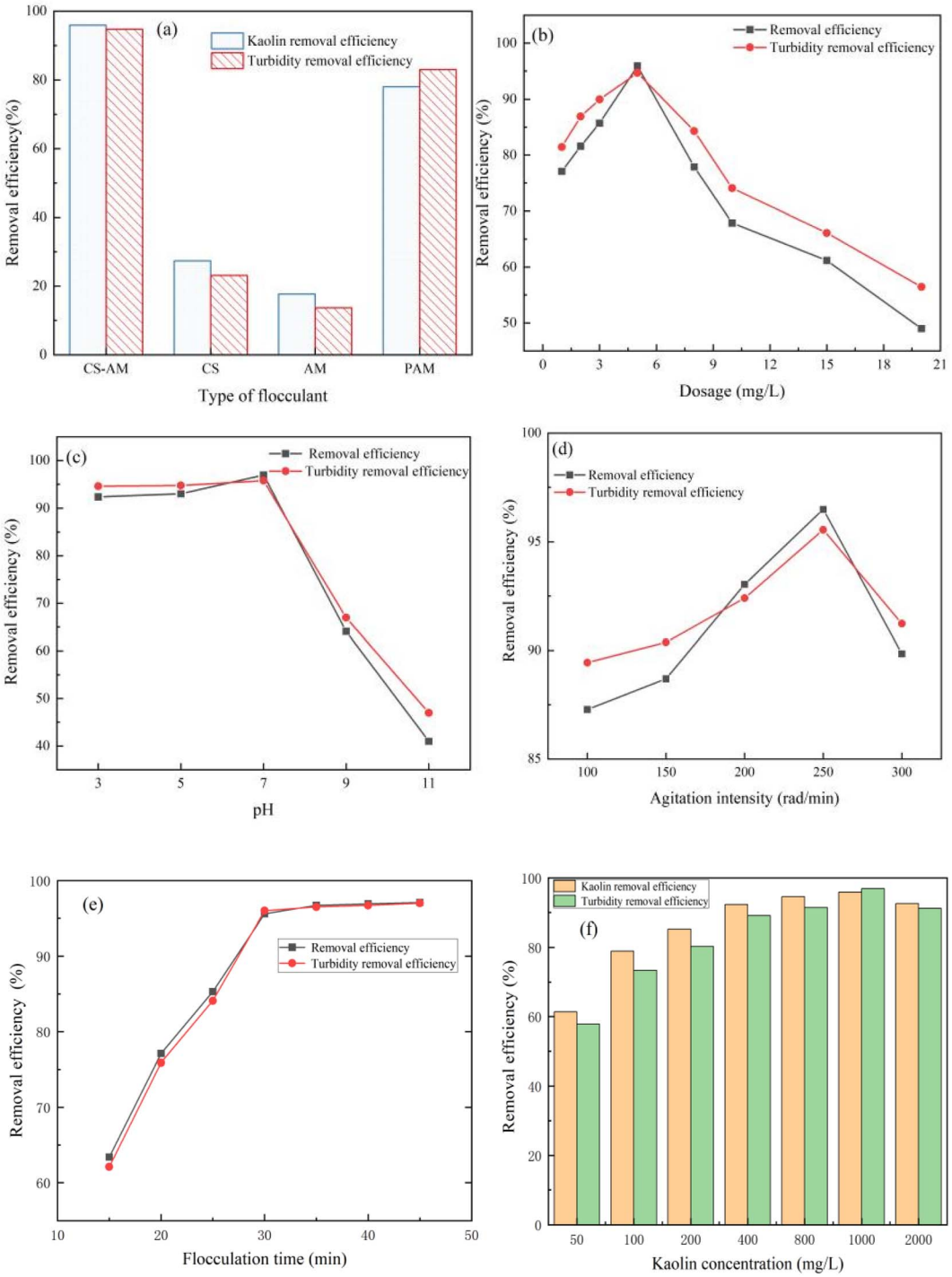

Fig. 9 (a) Removal of different flocculants on kaolin suspension; (b) effect of dosage on removal of kaolin suspension (pH = 7, stirring strength 250 rad per min, flocculation time 30 min, kaolin concentrations 1000 mg L^{-1}); (c) effect of pH on removal of kaolin suspension (flocculant 5 mg L^{-1}, stirring strength 250 rad per min, flocculation time 30 min, kaolin concentrations 1000 mg L^{-1}); (d) influence of stirring strength on removal of kaolin suspension (flocculant dosage 5 mg L^{-1}, pH = 7, flocculation time 30 min, kaolin concentrations 1000 mg L^{-1}); (e) removal efficiency of flocculation time (flocculant dosage 5 mg L^{-1}, pH = 7, kaolin concentrations 1000 mg L^{-1}, stirring strength 250 rad per min); (f) removal efficiency of different kaolin concentrations (flocculant dosage 5 mg L^{-1}, pH = 7, flocculation time 30 min, stirring strength 250 rad per min).

ions from the acid solution and groups on the flocculant promote uniform diffusion of the CS-AM molecular chain in water. This exposes the active sites of the molecular chain, facilitating collision with kaolin particles and enhancing flocculant adsorption and bridging.[54,55] As the pH increases, the ionization of amino groups in CS decreases, resulting in

a weakened ability to form NH_4^+. This diminishes the charge neutralization between CS and suspended particles, leading to a reduced flocculation effect.[56]

Fig. 9d illustrates the impact of stirring strength on the removal of kaolin suspension and turbidity. The figure reveals that, compared with flocculant dosage and solution pH, stirring strength has a relatively minor influence on the removal rate. However, overall, the removal decreases with increasing stirring strength, with optimal flocculation observed at a stirring strength of 250 rad per min. Mixing alters the hydrodynamic conditions within the solution, affecting the interaction between the flocculant and suspended particles. When the solution is stirred, the flow velocity in the fluid increases, leading to more frequent and intense collisions between the flocculant and suspended particles. This phenomenon promotes the binding of flocculants and particles, resulting in the formation of larger particle clusters and facilitating flocculation. However, excessively high agitation strength can have a counterproductive effect. Excessive agitation has the potential to disrupt the particle clusters, weakening or even nullifying the flocculant's effectiveness. Consequently, the stirring strength should be adjusted according to the specific circumstances to achieve the optimal flocculation effect.

Fig. 9e shows the influence of flocculation time on removal efficiency and turbidity of kaolin suspension. Too short flocculation time is not conducive to the growth and aggregation of tiny flocs after the mixed reaction of CS-AM and pollutants, so the removal efficiency of kaolin is low. To a certain extent, the extension of flocculation time is conducive to the collision and aggregation of microfloc and the growth of large floc particles, so as to improve the treatment effect. However, when the flocculation time is too long, not only can not improve the removal effect, but also may cause the floc particles to break due to the interaction between the floc, which makes the treatment effect worse. Therefore, the best flocculation time is 30 minutes.

In actual water treatment, the initial turbidity of wastewater is variable, which evidently influences the flocculation performance. As presented in Fig. 9f, the removal efficiency increased with increasing initial kaolin concentration and turbidity. In the range of 50–100 mg L^{-1}, the removal efficiency was relatively low, <80%. This is because the mean distance between particles was large, and the collision efficiency was not high enough. When the initial kaolin concentration and turbidity are high, the collision frequency and collision efficiency between particles increased, which could lead to a further increase in removal efficiency.[57] Even in the high turbidity kaolin suspension of 2000 mg L^{-1}, the removal efficiency of CS-AM can still reach 96.7%, indicating that CS-AM has excellent flocculation performance for kaolin.

CNTs suspension and the actual waste water flocculation and removal effect. The impact of the addition amount of CS-AM flocculant on the removal of CNTs and turbidity is depicted in Fig. 10a, and the optimal removal is achieved at 8 mg L^{-1}. Fig. 10b demonstrates the effect of solution pH on the removal of CNTs and turbidity, with higher removal rates observed in acidic solution environments, this is because at lower pH values, the H^+ ions in solution and negatively charged CNTs particles have partial electrical neutralization, and electrostatic attraction to make the flocculant and CNTs collision aggregation, which can greatly enhance the flocculation effect. In contrast, neutral and alkaline solution environments exhibit poorer removal effects for CNTs and turbidity, this is because with the increase of –OH number in the solution, the charge neutralization on the flocculant molecules weakens, and it can only rely on web coil sweep and adsorption bridge to trap CNTs particles, which leads to the reduction of flocculation performance. Moreover, as the pH increases, the number of negative charge on the surface of CNTs increased, and the repulsion between particles also increased, which inhibited the flocculation of CNTs. This suggests that the removal efficiency of CS-AM for CNTs and turbidity is more sensitive to changes in pH. Fig. 10c illustrates the effect of stirring strength on the removal of CNTs and turbidity. Stirring strength has minimal influence on the removal overall, with a trend of initially increasing and then decreasing as the stirring strength continues to rise. The optimal flocculation effect is achieved at a stirring strength of 250 rad per min. Fig. 10d shows the effect of flocculation time on the removal and turbidity of CNTs suspension. It can be seen that within thirty minutes, the removal rates of kaolin suspension and turbidity rapidly increase with time. But after 30 minutes, there is almost no change, so the optimal flocculation time is selected as 30 minutes.

In addition, the flocculation effects of CS-AM on three different types of actual wastewater were also investigated (Fig. S4†). A certain mass of concentration of kaolin was added into construction site wastewater, pharmaceutical wastewater, and domestic wastewater for flocculation treatment. It can be seen that CS-AM also had good effects on suspended solids removal from the actual wastewater. The higher the dosage of flocculant added during the treatment process, the higher the removal of pollutants. The COD removal efficiency in pharmaceutical wastewater was lower than in construction site wastewater and domestic wastewater. In practical applications, further research is needed on the optimal process parameters.

Zeta potential. Most of the water pollutants have a certain surface electrical property, and the positive and negative electrical properties have a great influence on the flocculation process. The charge property of the flocculant has an important influence on the flocculation effect and mechanism.[58] Studies show that the change of zeta potential means the flocculation dominated by general charge neutralization or adsorption bridging.[59]

Fig. 11 illustrates the change in zeta potential of the supernatant in the aqueous solution after the CS-AM reaction with kaolin and CNTs suspensions at different pH levels. The pH value of the aqueous solution significantly affects the zeta potential value after flocculation. In the case of the kaolin suspension, the zeta potential decreases as the pH increases. It exhibits positive values under neutral and acidic conditions and negative values under alkaline conditions. Similarly, for the CNTs nanoparticle suspension, the zeta potential of the supernatant decreases with increasing pH. It shows positive values under acidic conditions and negative values under neutral and alkaline conditions. These results align with the observed

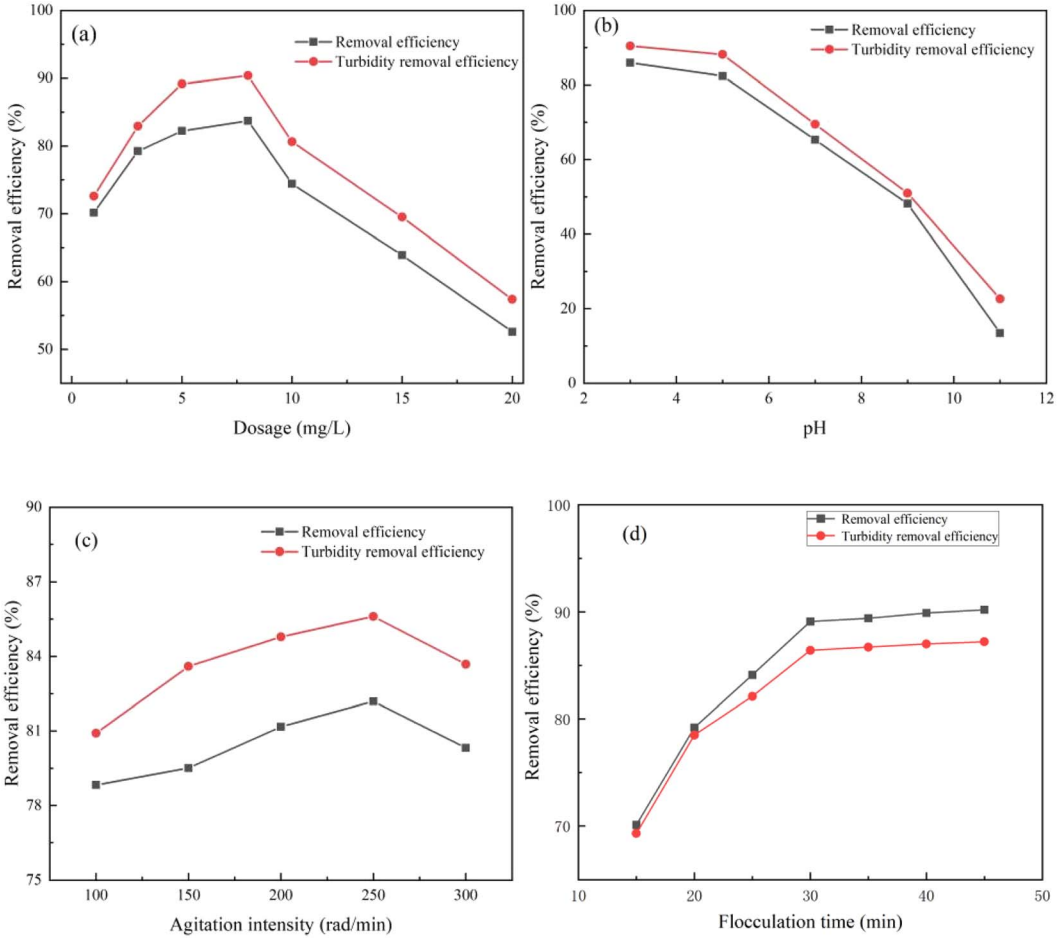

Fig. 10 (a) Solution for removal of CNTs and turbidity (pH = 5, stirring strength 250 rad per min, flocculation time 30 min); (b) effect of pH on CNTs and turbidity removal (addition amount of flocculant is 8 mg L^{-1}, stirring strength is 250 rad per min, flocculation time is 30 min); (c) effect of stirring strength on CNTs and turbidity removal (dosage of flocculant is 8 mg L^{-1}, pH = 5, flocculation time is 30 min); (d) effect of flocculation time on CNTs and turbidity removal (dosage of flocculant is 8 mg L^{-1}, pH = 5, stirring strength is 250 rad per min).

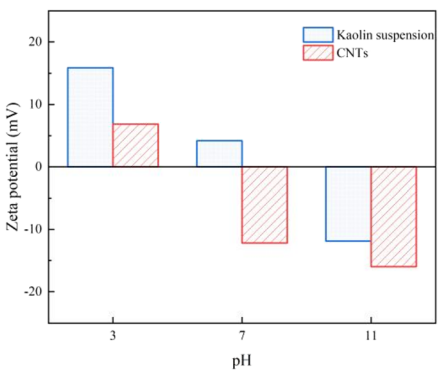

Fig. 11 Zeta potential changes with pH value.

pattern of zeta potential change in the solution after CS treatment with negatively charged pollutants in water, as reported by Zhang *et al.*,[60] under different pH conditions.

The above results suggest that CS-AM exhibits superior flocculation performance for kaolin suspension in acidic and neutral solution environments. FTIR characterization analysis indicates that amine groups and primary amine groups in CS-AM carry positive charges. Under acidic conditions, the flocculant exhibits a high positive charge density, leading to preferential charge neutralization with negatively charged kaolin particles.[61] However, even with an increase in pH, the zeta potential value of the kaolin suspension decreases, while the removal remains high. This result suggests that charge neutralization is not the sole mechanism responsible for kaolin particle removal. SEM analysis of CS-AM reveals its large specific surface area and porous structure, suggesting the involvement of adsorption bridging mechanisms in the flocculation process.[62] Furthermore, the grafting of AM increases the molecular weight of the flocculant, and studies indicate that high molecular weight flocculants exhibit more pronounced bridging effects. Therefore, the adsorption bridging effect of CS-AM during flocculation is also significant under different pH conditions.[60,63]

Conclusion

In this study, a chitosan-based flocculant, CS-AM, was prepared and synthesized by DBD plasma initiation synthesis. The best

conditions for the synthesis of CA-PAC were discharge time of 5 min, discharge power of 60 W, monomer mass concentration of 80 g L^{-1}, polymerization time of 3 h, polymerization temperature of 70 °C and m(CS) : m(AM) ratio of 1 : 3. The FTIR showed that CS-AM was prepared successfully. XRD showed that the crystal structure changed after AM grafted to CS, indicating that CS-AM was successfully prepared. The SEM showed that the surface morphology of CS-AM changed obviously, which was helpful to improve the flocculation performance. TG-DSC analysis revealed that CS-AM had good thermal stability. CS-AM showed remarkable flocculation effect on kaolin and carbon nanotube suspensions. Under acidic conditions, the removal of kaolin and carbon nanotube suspension by CS-AM mainly depended on charge neutralization. It has certain biodegradability and environmental friendliness, and has a good application prospect. DBD plasma provides a new method for the preparation and development of modified chitosan and broadens the application range of chitosan. However, how to improve the discharge reactor, make the discharge uniform, improve the energy efficiency and increase the yield of flocculant is an important direction of future research.

Author contributions

Haixia Wu contributed to the concept and design of manuscripts, supervised the research and reviewed the manuscript. The data analysis and first draft of manuscript was prepared by Wang Shen. Quanfa Zhao and Weiwei Zhang performed the experiments and data collection. All authors have read and approved the final manuscript.

Conflicts of interest

There are no conflicts to declare.

Acknowledgements

We acknowledge the grant from the National Natural Science Foundation of China (No. 51707093).

References

1 J. Li, Y. Q. Yun, L. Xing and L. Song, *Biosci., Biotechnol., Biochem.*, 2017, **81**, 1018–1025.
2 T. Zeng, X. Q. Hu, H. Wu, J. W. Yang and H. B. Zhang, *Int. J. Biol. Macromol.*, 2019, **131**, 760–768.
3 Q. F. Zhao, H. X. Wu, W. Shen, X. Han, B. Zheng B and J. F. Fan, *Plasma Sci. Technol.*, 2023, **25**, 104002.
4 Y. M. Ding, J. H. Zhao, L. Wei, W. P. Li and Y. P. Chi, *Appl. Sci.*, 2019, **9**, 973.
5 B. Z. Liu, H. L. Zheng, X. R. Deng, B. C. Xu, Y. J. Sun, Y. Z. Liu and J. J. Liang, *RSC Adv.*, 2017, **7**, 6114–6122.
6 J. L. Wang and S. T. Zhuang, *Crit. Rev. Environ. Sci. Technol.*, 2017, **47**, 2331–2386.
7 H. Hadiyanto, W. Widayat, M. Christwardana and M. E. Pratiwi, *Curr. Opin. Green Sustainable Chem.*, 2022, **5**, 100291.
8 K. Okaiyeto, U. U. Nwodo, S. A. Okoli, L. V. Mabinya and A. I. Okoh, *MicrobiologyOpen*, 2016, **5**, 177–211.
9 R. Yang, H. J. Li, M. Huang, H. Yang and A. M. Li, *Water Res.*, 2016, **95**, 59–89.
10 J. Chen, *Ultraviolet Light – H_2O_2 Study on 2-initiated Chitosan Based Modified Flocculant and its Application*, Kunming University of Science and Technology, 2021, (in Chinese).
11 J. Yu, J. D. Zheng, Q. F. Lu, S. X. Yang, X. Wang and X. M. Zhang, *J. Environ. Sci.*, 2017, **37**, 1003–1012.
12 W. X. Jiang, J. G. Han and H. Guo, *Sep. Purif. Technol.*, 2024, **330**, 125309.
13 B. Wang, N. Wang, Y. Sun, H. Xiao, M. Fu, S. Li, H. Liang, Z. Qiao and D. Ye, *Appl. Surf. Sci.*, 2022, **614**, 156162.
14 K. F. Shang, J. Li and R. Morent, *Plasma Sci. Technol.*, 2019, **21**, 043001.
15 K. F. Shang, R. Morent, N. Wang, Y. X. Wang, B. F. Peng, N. Jiang, N. Lu and J. Li, *Chem. Eng. J.*, 2022, **431**, 133916.
16 X. F. Zhou, H. F. Xiang, M. H. Yang, W. Q Geng and K. Liu, *J. Phys. D: Appl. Phys.*, 2023, **56**, 455202.
17 Y. Y. Su, Y. X. Yang, W. X. Jiang, J. G. Han and H. Guo, *Chem. Eng. J.*, 2023, **476**, 146469.
18 G. S. Oehrlein and S. Hamaguchi, *Plasma Sources Sci. Technol.*, 2018, **27**, 23001.
19 X. Lu, Y. H. Xu, W. Q. Sun, Y. J. Sun and H. L. Zheng, *Sci. Total Environ.*, 2017, **609**, 410–418.
20 W. Zou, L. Yu, X. X. Liu, L. Chen, X. Q. Zhang, D. L. Qiao and R. Z. Zhang, *Carbohydr. Polym.*, 2012, **87**, 1583–1588.
21 I. Sifuentes-Nieves, G. Velazquez, P. C. Flores-Silva, E. Hernández-Hernández, G. Neira-Velázquez, C. Gallardo-Vega and G. Mendez-Montealvo, *Int. J. Biol. Macromol.*, 2020, **144**, 682–689.
22 Y. J. Sun, C. Y. Zhu, W. Q. Sun, Y. H. Xu, X. F. Xiao, H. L. Zheng, H. F. Wu and C. Y. Liu, *Carbohydr. Polym.*, 2017, **164**, 222–232.
23 Y. W. Wang, W. X. Jiang, J. D. Han, W. C. Qiao and H. Guo, *Chemosphere*, 2023, **333**, 138958.
24 T. R. Kiran, K. S. Vinai, K. S. Manoj, S. Krishnamoorthi and K. Krishna, *Polym. J.*, 2020, **29**, 615–623.
25 O. Carton, D. B. Salem, J. Pulpytel and F. Arefi-Khonsari, *Plasma Chem. Plasma Process.*, 2015, **35**, 819–829.
26 D. Wang, X. Xie, J. Jow, H. Y. Chen and S. Y. Lai, *J. Appl. Polym. Sci.*, 2008, **108**, 1737–1743.
27 S. L. Peng, G. C. Jiang, X. L. Li, L. L. Yang, F. Liu and Y. B. He, *J. Chem. Technol. Biotechnol.*, 2018, **93**, 968–974.
28 P. Wu, J. X. Yi, L. Feng, X. H. Li, Y. M. Chen, Z. Liu, S. H. Tian, S. Y. Li, S. Khan and Y. J. Sun, *Int. J. Biol. Macromol.*, 2020, **155**, 708–720.
29 K. Kiran, R. Tiwari, K. Tungala, S. Krishnamoorthi and K. Kumar, *Global Chall.*, 2020, **4**, 1900089.
30 R. Mpon, M. K. Ndikontar, H. N. Ntede, J. N. Ngamveng, A. Dufresne, O. Ayina, E. Njungap and A. Tame, *J. Med. Chem.*, 2012, **9**, 373–380.
31 H. L. Zheng, Y. J. Sun, C. J. Zhu, J. S. Guo, C. Zhao, Y. Liao and Q. Q. Guan, *Chem. Eng. J.*, 2013, **234**, 318–326.
32 H. L. Zheng, Y. L. Sun, J. S. Guo, F. T. Lo, W. Fan, Y. Liao and Q. Q. Guan, *Ind. Eng. Chem. Res.*, 2014, **53**, 2572–2582.

33 K. Kiran, R. Tiwari, K. Tungala, S. Krishnamoorthi and K. Kumar, *J. Polym. Res.*, 2020, **27**, 1–11.
34 J. P. Wang, Y. Z. Chen, S. J. Yuan, G. P. Sheng and H. Q. Yu, *Water Res.*, 2009, **43**, 5267–5275.
35 F. A. Razmi, N. Ngadi, S. Wong, L. M. Inuwa and L. A. Opotu, *J. Cleaner Prod.*, 2019, **231**, 98–109.
36 N. Gomathi, R. Rajasekar, R. R. Babu, D. Mishra and S. Neogi, *Mater. Sci. Eng., C*, 2012, **32**, 1767–1778.
37 S. Li, K. Q. Han, H. P. Rong, X. Z. Li and M. H. Yu, *J. Appl. Polym. Sci.*, 2014, **131**, 40250.
38 X. Li, H. L. Zheng, Y. L. Wang, Y. J. Sun, B. C. Xu and C. L. Zhao, *Chem. Eng. J.*, 2017, **319**, 119–130.
39 Y. J. Sun, M. J. Ren, W. Q. Sun, X. F. Xiao, Y. H. Xu, H. L. Zheng, H. F. Wu, Z. Y. Liu and H. Zhu, *Environ. Sci. Technol.*, 2019, **40**, 954–968.
40 D. B. Zakaria, H. L. Zheng, M. X. Wang, S. Liu, X. M. Tang, S. Khan, A. N. Jimené and L. Feng, *Int. J. Polym. Sci.*, 2018, **2018**, 1–12.
41 J. Y. Ma, W. Xia, R. Zhang, L. Ding, Y. Kong, H. W. Zhang and K. Fu, *J. Hazard. Mater.*, 2021, **403**, 123690.
42 B. Z. Liu, X. Chen, H. L. Zheng, Y. L. Wang, Y. J. Sun, C. L. Zhao and S. X. Zhang, *Carbohydr. Polym.*, 2018, **181**, 327–336.
43 B. Z. Liu, H. L. Zheng, Y. L. WangL, X. Chen, C. L. Zhao and Y. Y. An, *Sci. Total Environ.*, 2018, **640–641**, 107–115.
44 Y. Z. Liu, H. L. Zheng, Y. Y. An, J. Ren, X. Y. Zheng, C. Zhao and S. Y. Zhang, *Sep. Purif. Technol.*, 2019, **228**, 115735.
45 Y. Z. Liu, H. L. Zheng, Y. J. Sun, J. Ren, X. Y. Zheng, Q. Sun, S. J. Jiang and W. Ding, *J. Cleaner Prod.*, 2020, **249**, 119350.
46 P. O. Boamah, Y. Huang, M. Q. Hua, Q. Zhang, Y. Y. Liu, J. Onumah, W. Wang and Y. X. Song, *Carbohydr. Polym.*, 2015, **122**, 255–264.
47 Y. Wu, Y. L. Zheng, W. L. Yang, C. C. Wang, J. H. Hu and S. K. Fu, *Carbohydr. Polym.*, 2005, **59**, 165–171.
48 Y. J. Sun, M. J. Ren, C. Y. Zhu, Y. H. Xu, H. L. Zheng, X. F. Xiao, H. F. Wu, T. Xia and Z. Y. You, *Ind. Eng. Chem. Res.*, 2016, **55**, 10025–10035.
49 Q. T. Lin, H. L. Peng, S. X. Zhong and J. X. Xiang, *J. Hazard. Mater.*, 2015, **285**, 199–206.
50 Z. Yang, H. J. Li, H. Yan, H. Wu, H. Yang, Q. Wu, H. P. Li, A. M. Li and R. S. Cheng, *J. Hazard. Mater.*, 2014, **276**, 480–488.
51 W. X. Jin, J. Nan, M. Chen, L. R. Song and F. M. Wu, *J. Hazard. Mater.*, 2023, **452**, 131273.
52 J. Y. Ma, J. Shi, H. C. Ding, G. C. Zhu, K. Fu and X. Fu, *Chem. Eng. J.*, 2017, **312**, 20–29.
53 J. Majeed, J. Ramkumar, S. Chandramouleeswaran and A. K. Tyagi, *Sep. Sci. Technol.*, 2015, **50**, 404–410.
54 J. Zhang, G. H. Guan, T. Lou and X. J. Wang, *Starke*, 2021, **73**, 2100047.
55 J. Kang and R. A. McLaughlin, *J. Polym. Environ.*, 2020, **28**, 1335–1343.
56 H. Maruyama, H. Seki and A. Igi, *Biochem. Eng. J.*, 2020, **162**, 107713.
57 J. Li, S. Jiao, L. Zhong, J. Pan and Q. Ma, *Colloids Surf., A*, 2013, **428**, 100–110.
58 Z. W. Lin, C. H. Zhang, Y. F. Hu, P. D. Su, B. X. Quan, X. Z. Li and Z. Zhang, *J. Cleaner Prod.*, 2023, **399**, 136582.
59 Y. J. Sun, Y. Y. Yu, X. Zheng, A. W. Chen and H. L. Zheng, *Carbohydr. Polym.*, 2021, **261**, 117891.
60 S. Zhang, T. Lu, D. Qi and H. Zhao, *J. Dispersion Sci. Technol.*, 2017, **38**, 1049–1054.
61 M. X. Wang, L. Feng, X. Y. You and H. L. Zheng, *Chemosphere*, 2021, **264**, 128525.
62 M. Wang, L. Yue, S. B. Niazi, I. M. Khan, Y. Zhang and Z. P. Wang, *Int. J. Biol. Macromol.*, 2022, **206**, 886–895.
63 J. S. Cui, X. J. Niu, D. Q. Zhang, J. L. Ma, X. F. Zhu, X. X. Zheng, Z. Lin and M. L. Fu, *Carbohydr. Polym.*, 2023, **304**, 120474.